Density Functional Study of Platinum(II)-Mediated Bicyclization of 1,6-Dienylphenols

Taraneh Nowroozi-Isfahani, Djamaladdin G. Musaev,* and Keiji Morokuma*

Cherry L. Emerson Center for Scientific Computation and Department of Chemistry, Emory University, Atlanta, Georgia 30322

Michel R. Gagné

Department of Chemistry, University of North Carolina at Chapel Hill, Chapel Hill, North Carolina 27599-3290

Received July 13, 2006

Density functional studies of the cyclization of a 1,6-dienylphenol by a Pt(II)-pincer complex were performed to better understand the mechanism of the bicyclization reaction. Of the four different diastereomers of the reaction's final product, the isomer resulting from the chairlike transition state that places the activated alkene in a pseudo-equatorial orientation was found to be the most stable, in agreement with experimental observations. The study of reaction mechanism concludes that the bicyclization proceeds in the presence of base via a concerted path with no significant barrier, while the stepwise path involving a discrete carbocationic intermediate seems less favorable.

1. Introduction

Discovery of the first biomimetic enantioselective cyclization of simple polyenes to polycyclic isoprenoids using Lewis acid assisted chiral Brønsted acids (LBA's) by Yamamoto and co-workers[1] has reignited the search for catalysts for nonenzymatic cation−olefin cyclization reactions. Early studies in this area focused on soft electrophilic metals that activated the electron-rich trisubstituted alkenes (e.g., Hg(II)).[2] More recently, however, efforts have shifted toward metals that prefer to coordinate and activate the less substituted alkene. In this regard Pt(II) and especially Pd(II) have well-deserved reputations as synthetically useful catalysts for olefin activation. Numerous studies have demonstrated that transition-metal catalysts (mainly Pd and Pt) can be used to activate electron-rich alkenes to initiate steroidlike cation−olefin cascades of polyprenoids, and the coordination of alkene nucleophiles to M(II)−alkene intermediates is a vital step of that process.[3−6] Both experimental and theoretical studies have revealed that increasing the positive charge on the transition-metal center enhances the electrophilicity of the coordinated alkene and facilitates addition reactions.[7] Dicationic transition-metal complexes should therefore display an exceptionally high reactivity toward nucleophilic attack on the coordinated alkene. However, the existence of β-H elimination pathways complicates the use of many existing dicationic transition-metal complexes, since this reaction can prematurely break the M−C bond.[2]

In this aspect, the recently synthesized dicationic monoalkene complexes of $(PNP)Pd^{2+}$ and $(PPP)Pt^{2+}$ (PNP = 2,6-bis-((diphenylphosphino)methyl)pyridine, and PPP = bis(2-(diphenylphosphanyl)ethyl)phenylphosphane)[8] are very promising. Indeed, the pincer ligands (PNP and PPP) bear no open cis coordination site on the metal, so that the undesirable β-hydride elimination process is inhibited. Gagné and co-workers have recently trapped the putative intermediate from electrophilic carbocyclization of 1,5- and 1,6-dienes.[3] The reaction of interest for the present theoretical study is the bicyclization of 1,6-dienylphenol in the presence of $(PPP)Pt^{2+}$, shown in Scheme 1.[3] According to the experimental evidence,[3] the $(PPP)Pt^{2+}$ catalyst is thought to coordinate the least substituted alkene and convert the dienylphenol into a diastereomeric pair of new metal-containing products (**INTb**$^+$) in the presence of a weak base. Further reductive cleavage of **INTb**$^+$ in the presence of $NaBH_4$ produces the tricyclic products with 86% yield. X-ray studies of the major isomer confirmed the relative configuration shown in Scheme 1. It is believed that this major isomer results from a chairlike transition state that places the activated alkene in a pseudo-equatorial orientation. Surprisingly, the minor product (14%) also contains a trans ring junction, but a Me−Me NOE (nuclear Overhauser effect) suggested a 1,3-diaxial disposition arising from a pseudoaxial positioning in the putative transition state.

The mechanism and factors controlling this process, however, are still unknown. Although the data ((*E*)-alkene going to trans ring junction) suggested a concerted process without a discrete carbocation (a mechanism for forming a cis ring junction), unambiguous discrimination between these two possibilities was not possible with the available data. The two limiting mechanisms are described in Scheme 1, with the stepwise mechanism proceeding through intermediate **INTa**$^{2+}$, which has no C−O

* To whom correspondence should be addressed. E-mail: dmusaev@emory.edu (D.G.M.); morokuma@emory.edu (K.M.).

(1) Nakamura, S.; Ishihara, K.; Yamamoto, H. *J. Am. Chem. Soc.* **2000**, *122*, 8131−8140.

(2) (a) Nishizawa, M.; Takenaka, H.; Hayashi, Y. *J. Org. Chem*, **1986**, *51*, 806−13. (b) Nishizawa, M.; Takenaka, H.; Hayashi, Y. *J. Am. Chem. Soc.* **1985**, *107*, 522−3.

(3) Koh, J. H.; Gagne, M. R. *Angew. Chem., Int. Ed.* **2004**, *43*, 4828−4828.

(4) Kerber, W. D.; Koh, J. H.; Gagne, M. R. *Org. Lett.* **2004**, *6*, 3013−3015.

(5) Kerber, W. D.; Gagne, M. R. *Org. Lett.* **2005**, *7*, 3379−3381.

(6) Koh, J. H.; Mascarenhas, C.; Gagné, M. R. *Tetrahedron* **2004**, *60*, 7405−7410.

(7) Hahn, C.; Morvillo, P.; Herdtweck, E.; Vitagliano, A. *Organometallics* **2002**, *21*, 1807−1818.

(8) Hahn, C.; Cucciolito, M. E.; Vitagliano, A. *J. Am. Chem. Soc.* **2002**, *124*, 9038−9039.

10.1021/om060632f CCC: $37.00
Publication on Web 04/06/2007

Scheme 1. Cyclization of 1,6-Dienylphenol in the Presence of $(PPP)Pt^{2+}$ [a]

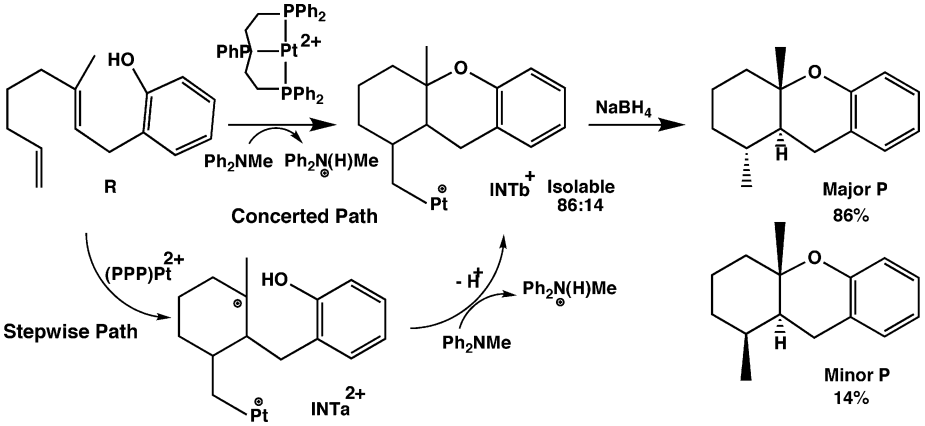

[a] PPP = bis(2-(diphenylphosphanyl)ethyl)phenylphosphane.

bond, while the concerted pathway is assumed to proceed through a transition state with at least partial bonding between the tertiary carbon and the oxygen of the phenol. The mechanism of this reaction, as well as the structure and stability of the proposed intermediates and transition states, remains to be elucidated.

To gain insight into the mechanism of the $(PPP)Pt^{II}$-mediated bicyclization of 1,6-dienylphenol, as well as address the possibility of forming carbocationic intermediates during the reaction, we have performed density functional studies of the mechanism of this reaction and herein report our results. We hope these insights will help design new and more efficient catalysts for enantioselective cation−olefin cyclizations. To the best of our knowledge, this is the first computational study on the Pt-mediated cyclization of polyenes, although several studies have been reported on ene−yne cycloisomerizations with $PtCl_2$.[9] Not to be forgotten are seminal computational studies on enzymatic cation−olefin cyclization of 2,3-oxidosqualene to lanosterol (a tetracyclic ring (A−D) system of steroids), which support a concerted mechanism for the oxirane cleavage and A/B ring formation.[10−12] However, a more recent study indicates the existence of two shallow minima for cyclic carbocations on the chair−boat path of the A/B ring closure.[13] Furthermore, in another report, a concerted A/B ring closure for the cyclization of squalene to hopene is suggested.[14]

2. Computational Procedure

All calculations were performed using the hybrid density functional B3LYP[15] in conjunction with the standard Lanl2dz + d(P) basis set,[16] which combines the Hay−Wadt relativistic effective core potential (ECP) and associated valence double-ζ basis set for Pt and the 6-31G(dP) basis set for main-group elements, which is 6-31G supplemented with a set of polarization d functions (α = 0.364)[17] for P atoms. Previously it was reported that the B3LYP/Lanl2dz+6-31G(dP) approach reasonably describes the analogous systems.[18]

In the present study we have adopted two models for the catalyst $PhP(CH_2CH_2PPh_2)_2Pt^{2+}$ ($(PPP)Pt^{2+}$; PPP = bis(2-(diphenylphosphanyl)ethyl)phenylphosphane) used in the experiment.[3] One of them, $HP(CH_2CH_2PH_2)_2Pt^{2+}$, is relatively small and has each of the phenyl groups replaced by hydrogen atoms. Most of the calculations were carried out using this small model of the catalyst because of the high computational cost of the proposed intermediates and transition states. In several cases (see below for more details) we also used a larger model of the catalyst, $HP(CH_2CH_2PPh_2)_2Pt^{2+}$, which includes four phenyl groups of the pincer ligand in the calculations. In most cases, the experimentally used substrate, $CH_2{=}CH(CH_2)_3MeC{=}CHCH_2PhOH$, was modeled by the simplified $CH_2{=}CH(CH_2)_3MeC{=}CHCH_2CH{=}CHOH$: i.e. by replacing the phenyl group with a vinyl group. In several cases, the real substrate was used. The base, Ph_2NMe, has been modeled by NMe_3.

Harmonic vibration frequency (unscaled) calculations were performed for each optimized structure to identify its nature as well as to include the thermal and entropy contributions to the calculated energies. Throughout the paper, energies presented without parentheses are enthalpies, and those in parentheses are Gibbs free energies at 298.15 K and 1 atm unless otherwise stated. Also, to confirm the connectivity of reactants and products, we have performed pseudo-IRC calculations[19] (a few steps of IRC followed by optimization) from transition-state structures. The bulk-solvent effects were evaluated at the polarizable continuum model (PCM)[20] level using the gas-phase optimized structures. As in the experiment, dichloromethane was used as the solvent media. Zero-point energy,

(9) (a) Marco-Contelles, J.; Soriano, E. *THEOCHEM* **2006**, *761*, 45−51. (b) Soriano, E.; Ballesteros, P.; Marco-Contelles, J. *Organometallics* **2005**, *24*, 3182−3191. (c) Soriano, E.; Ballesteros, P.; Marco-Contelles, J. *Organometallics* **2005**, *24*, 3172−3181.

(10) Jenson, C.; Jorgensen, W. L. *J. Am. Chem. Soc.* **1997**, *119*, 10846−10854.

(11) Gao, D.; Pan, Y. K. *J. Am. Chem. Soc.* **1998**, *120*, 4045−4046.

(12) Hess, B. A., Jr. *Collect. Czech. Chem. Commun.* **2003**, *68*, 202.

(13) Hess, B. A., Jr.; Smentek, L. *Mol. Phys.* **2004**, *102*(11−12), 1201−1206.

(14) Hess, B. A., Jr.; Smentek, L. *Org. lett.* **2004**, *6*(11), 1717−1720.

(15) (a) Becke, A. D. *J. Chem. Phys.* **1993**, *98*, 1372−1380. (b) Lee, C.; Yang, W.; Parr, R. G. *Phys. Rev. B* **1998**, *37*, 785−789.

(16) (a) Dunning, J., T. H.; P. J. In *Modern Theoretical Chemistry*, Ed. Schaefer, H. F., III, Ed.; Plenum: New York, 1976; pp 1−28. (b) Hay, P. J.; Wadt, W. R. *J. Chem. Phys.* **1985**, *82*, 270−283. (c) Wadt, W. R.; Hay, P. J. *J. Chem. Phys.* **1985**, *82*, 284−298. (d) Hay, P. J.; Wadt, W. R. *J. Chem. Phys.* **1985**, *82*, 299−310.

(17) http://www.emsl.pnl.gov/forms/basisform.html.

(18) (a) Cui, Q.; Musaev, D. G.; Svensson, M.; Sieber, S.; Morokuma, K. *J. Am. Chem. Soc.* **1995**, *117*, 12366−12367. (b) Musaev, D. G.; Morokuma, K. *J. Phys. Chem.* **1996**, *100*, 6509−6517. (c) Erikson, L. A.; Pettersson, L. G. M.; Siegbahn, P. E. M.; Wahlgren, U. *J. Chem. Phys.* **1995**, *102*, 872−878. (d) Ricca, A.; Bauschlicher, C. W., Jr. *J. Phys. Chem.* **1994**, *98*, 12899−12903. (e) Heinemann, C.; Hertwig, R. H.; Wesendrup, R.; Koch, W.; Schwarz, H. *J. Am. Chem. Soc.* **1995**, *117*, 495−500. (f) Hertwig, R. H.; Hrusak, J.; Schroder, D.; Koch, W.; Schwarz, H. *Chem. Phys. Lett.* **1995**, *236*, 194−200. (g) Schroder, D.; Hrusak, J.; Hertwig, R. H.; Koch, W.; Schwerdtfeger, P.; Schwarz, H. *Organometallics* **1995**, *14*, 312−316. (h) Fiedler, A.; Schroder, D.; Shaik, S.; Schwarz, H. *J. Am. Chem. Soc.* **1994**, *116*, 10734−10741. (i) Fan, L.; Ziegler, T. *J. Chem. Phys.* **1991**, *95*, 7401−7408. (j) Berces, A.; Ziegler, T.; Fan, L. *J. Phys. Chem.* **1994**, *98*, 1584−1595. (k) Lyne, P. D.; Mingos, D. M. P.; Ziegler, T.; Downs, A. J. *Inorg. Chem.* **1993**, *32*, 4785−4796. (l) Li, J.; Schreckenbach, G.; Ziegler, T. *J. Am. Chem. Soc.* **1995**, *117*, 486−494.

(19) Fukui, K. *Acc. Chem. Res.* **1981**, *14*, 363.

(20) (a) Tomasi, J.; Persico, M. *Chem. Rev.* **1994**, *94*, 2027−2094. (b) Cammi, R.; Tomasi, J. *J. Comput. Chem.* **1996**, *16*, 1449−58.

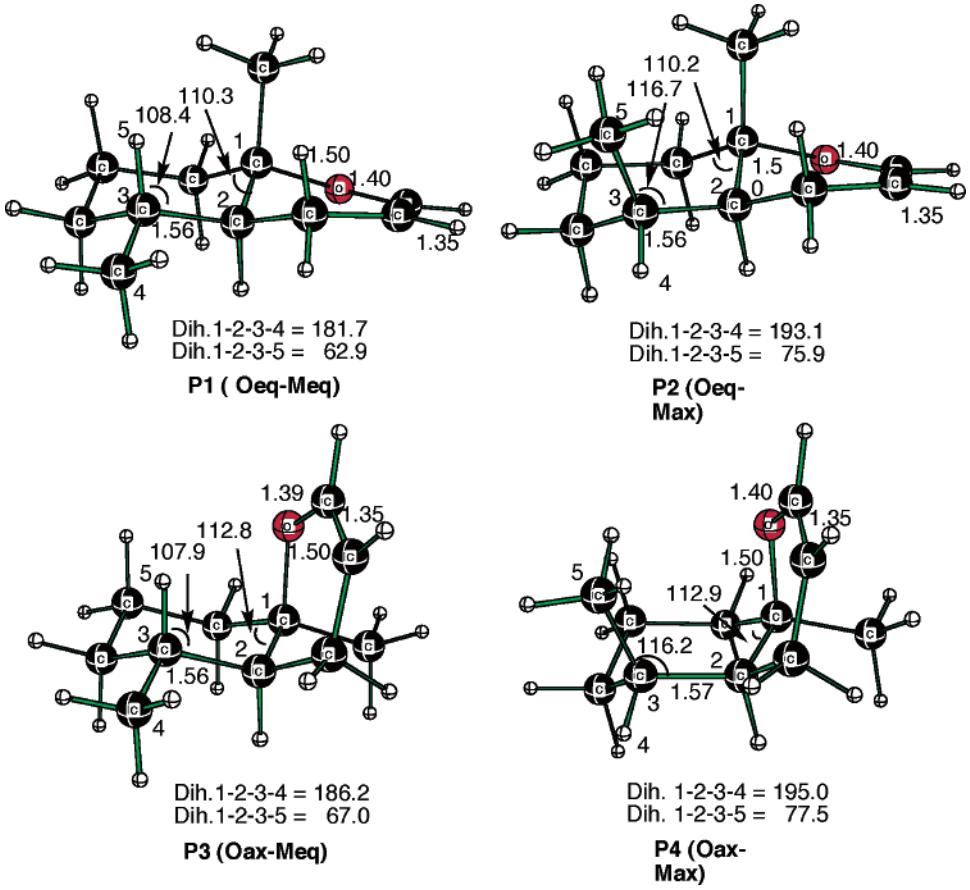

Figure 1. Calculated geometrical structures (with bond distances in Å) of the four different diastereoisomers of the product **P** (model). The number 5 always refers to the axial position, regardless of the atom type.

enthalpy, and Gibbs free energy corrections were estimated from the gas-phase studies and included in the PCM-calculated solvation energy. The standard natural population analysis (NPA)[21] was performed to calculate the atomic charges. All calculations were performed without symmetry constraints utilizing the Gaussian_03 program.[22]

Throughout the paper, we use the following nomenclature to refer to relevant species: **R** for reactants, **INTa**$^{2+}$ and **INTb**$^{+}$ for the two putative intermediates (discussed in the Introduction), **TS** for transition states, and **P** for products. Each of these structures (to be discussed in section 3A) may have four isomers, **1 (Oeq-Meq)**, **2** (**Oeq-Max)**, **3** (**Oax-Meq)**, and **4** (**Oax-Max)**, which is denoted as **Xn**, where **X** = **R**, **INT**, **TS**, **P**, and **n** = **1**−**4**. These isomers differ by the *eq*uatorial and *ax*ial positioning of the *O*H and the *exo-M*ethyl group. For instance, **Oeq-Meq** is an isomer with both *O*H and *exo-M*ethyl in the *eq*uatorial position (for example, see Figure 1). Obviously, the axial−equatorial nomenclature has no meaning for **R1**−**R4**, which represent four conformers of **R** preorganized to generate the corresponding **P1**−**P4** structures. Throughout the paper, **R1** leading to the experimental major isomer **P1** is considered as the reference for the calculation of relative energies. We also use L−(PPP)Pt^{2+} **(**where L = NMe_3, CH_2Cl_2, CH_2═CH_2, CH_2═CHMe) to refer to possible complexes of the catalyst with base, solvent, and olefin. Complexes of (CH_2═CH_2)(PPP)Pt^{2+} and (CH_2═CHMe)(PPP)Pt^{2+} may have two isomers, coplanar and out of plane, which are denoted as **Iso-1** and **Iso-2**, respectively.

3. Results and Discussion

As mentioned in the introduction, two stereoisomers of the product **P** have a trans ring junction. These isomers differ by the positioning of the activated alkene in the cyclization reaction; it is located in a pseudo-equatorial orientation in the case of the major isomer **P1** and in a pseudoaxial position for the minor isomer **P2**. For the sake of completeness, we also discuss isomers **P3** and **P4**, which could be produced by a cis ring junction, again placing the activated alkene in a pseudo-equatorial orientation **P3** or a pseudo-axial **P4** position. To have a better view of the differences between these isomers, we first report in section A our computational results on the thermodynamics of the reaction, comparing the structures and relative stabilities of the four stereoisomers of key species **P**, **INTb**$^{+}$, and **INTa**$^{2+}$. In section B, we discuss the reaction mechanism for the path that leads to the major isomer **P1** and a subset of the path for the minor isomer **P2**. In section C, the effect of bulk solvent is reported.

A. Thermodynamics of Possible Product and Intermediate Stereoisomers. The optimized structures for four stereoisomers

(21) Reed, A. E.; Weinstock, R. B.; Weinhold, F. *J. Chem. Phys.* **1985**, *83*, 735−746.

(22) Frisch, M. J.; Trucks, G. W.; Schlegel, H. B.; Scuseria, G. E.; Robb, M. A.; Cheeseman, J. R.; Montgomery, J. A., Jr.; Vreven, T.; Kudin, K. N.; Burant, J. C.; Millam, J. M.; Iyengar, S. S.; Tomasi, J.; Barone, V.; Mennucci, B.; Cossi, M.; Scalmani, G.; Rega, N.; Petersson, G. A.; Nakatsuji, H.; Hada, M.; Ehara, M.; Toyota, K.; Fukuda, R.; Hasegawa, J.; Ishida, M.; Nakajima, T.; Honda, Y.; Kitao, O.; Nakai, H.; Klene, M.; Li, X.; Knox, J. E.; Hratchian, H. P.; Cross, J. B.; Bakken, V.; Adamo, C.; Jaramillo, J.; Gomperts, R.; Stratmann, R. E.; Yazyev, O.; Austin, A. J.; Cammi, R.; Pomelli, C.; Ochterski, J. W.; Ayala, P. Y.; Morokuma, K.; Voth, G. A.; Salvador, P.; Dannenberg, J. J.; Zakrzewski, V. G.; Dapprich, S.; Daniels, A. D.; Strain, M. C.; Farkas, O.; Malick, D. K.; Rabuck, A. D.; Raghavachari, K.; Foresman, J. B.; Ortiz, J. V.; Cui, Q.; Baboul, A. G.; Clifford, S.; Cioslowski, J.; Stefanov, B. B.; Liu, G.; Liashenko, A.; Piskorz, P.; Komaromi, I.; Martin, R. L.; Fox, D. J.; Keith, T.; Al-Laham, M. A.; Peng, C. Y.; Nanayakkara, A.; Challacombe, M.; Gill, P. M. W.; Johnson, B.; Chen, W.; Wong, M. W.; Gonzalez, C.; Pople, J. A. *Gaussian 03*, revision C.02; Gaussian, Inc.: Wallingford, CT, 2004.

Table 1. Relative Enthalpy and Gibbs Free Energy (in Parentheses) (in kcal/mol at 298.15 K and 1 atm) of the Four Possible Isomers of Reactant R, Intermediates $INTa^{2+}$ and $INTb^{+}$, and Products P, with Respect to the Isomer 1 (Oeq-Meq), Which Was Experimentally Observed

	complex			
	1 (Oeq-Meq)	**2 (Oeq-Max)**	**3 (Oax-Meq)**	**4 (Oax-Max)**
R	0.00 (0.00)	2.52 (1.73)	0.58 (−0.94)	0.33 (1.16)
$INTa^{2+}$	0.00 (0.00)	4.10 (4.41)	3.21 (3.23)	6.51 (7.45)
$INTb^{+}$	0.00 (0.00)	4.00 (4.73)	−1.04 (0.10)	1.12 (1.90)
P	0.00 (0.00)	3.83 (3.90)	0.05 (−0.04)	3.55 (3.97)
P-Large	0.00 (0.00)	3.70 (3.49)	−0.15 (−0.31)	3.19 (3.69)

of **P** are given in Figure 1, showing their important geometrical parameters; their relative energies are collected in Table 1. As seen in Table 1, the energetically most stable isomers are **P1** and **P3**. These results are in good agreement with the X-ray data indicating **P1** as the major diastereomer and **P2** as a minor product. The relative stability of these isomers can be explained by the steric repulsion between the methyl groups, which is larger in **P2** and **P4** than in **P1** and **P3**. To determine the effect of methyl−methyl and methyl−heterocycle 1,3-steric repulsion in **P2** and **P4**, respectively, we carried out single-point energy calculations of **P2** at the **P1** geometry (with notation **P2//P1)** and **P4** at the **P3** geometry (**P4//P3**). The obtained energy difference between **P2//P1** and **P1//P1** is 13.0 kcal/mol, and that between **P4**//**P3** and **P4**//**P4** is 14.7 kcal/mol. Figure 1 shows that structures **P2** and **P4** have adjusted dihedral angles to reduce steric repulsion.

To test the reliability of the aforementioned results obtained by utilizing the smaller model CH_2═$CH(CH_2)_3MeC$═$CHCH_2$-CH═CHOH (denoted as **P**), we optimized the structure of the four stereoisomers of the experimentally used substrate CH_2═$CH(CH_2)_3MeC$═$CHCH_2PhOH$, denoted as **P-Large**, which explicitly includes the phenyl group in the calculations. The important geometrical parameters and the relative energies are shown in Figure S1 of the Supporting Information and in Table 1, respectively. A comparison of the calculated geometries for model structures **P** and **P-Large** indicate that the C═C bonds in **Pn** structures are ca. 0.06 Å shorter than those in their **P-Large** analogues. Changes in other geometrical parameters, especially those involved in the course of the reaction, are insignificant. The relative energies of **P** and **P-Large** isomers (Table 1) are very similar: i.e., isomers **P1** and **P3** are more stable by ca. 3.5 kcal/mol than **P2** and **P4**. Therefore, we conclude that the small model used in this paper provides reliable data.

Next, we located two sets of intermediates, **$INTa^{2+}$** and **$INTb^{+}$,** for each of the four diastereomers. As mentioned above, **$INTa^{2+}$**, with one ring already formed and a tertiary carbocation interacting with the hydroxyl group, is almost certainly on the stepwise pathway to **$INTb^{+}$**, an intermediate which is experimentally isolated.[3] The optimized structures of four different stereoisomers of **$INTb^{+}$** and **$INTa^{2+}$** are shown in Figure 2. The results show that, on going from **$INTan^{2+}$** to **$INTbn^{+}$** (where **n** = **1**−**4**), the C···O(H) distance is reduced from 1.64−1.66 to 1.49−1.50 Å. As a consequence, the adjacent HO−C bond is also shortened from 1.46−1.47 to 1.40 Å. A comparison of the calculated geometrical parameters of **$INTbn^{+}$** with the corresponding products **Pn** confirms that the cyclization is indeed completed when the intermediate **$INTb^{+}$** is formed.

The relative energies shown in Table 1 indicate that, for both intermediates **$INTa^{2+}$** and **$INTb^{+}$**, the most stable isomers are **1** and **3**, similar to the product (**P**) case, and the 1,3-diaxial isomer **2** is energetically less favorable by about 4.0 kcal/mol with respect to isomer **1**. Interestingly, the cis ring junction isomers **3** and **4** are significantly stabilized upon deprotonation of **$INTa^{2+}$** to **$INTb^{+}$**, as compared to trans ring junction isomers **1** and **2**. Our careful comparison of the structures utilizing single-point calculations of the catalyst and alkene fragments do not show a significant change in structures and relative energies of the fragments. Thus, we believe that subtle interactions between these two fragments could be the cause of the difference.

As explained in the Computational Procedure, four preorganized conformers of the reactant **R** were also optimized; the geometrical parameters are provided in Figure S2 of the Supporting Information. Here, one should note that the thermodynamics of the reaction **R** + $(PPP)Pt^{2+}$ → **$INTa^{2+}$** → **$INTb^{+}$** + H^{+} → **P** + $(PPP)Pt^{2+}$ are very similar for the four conformers; the overall exothermicities of the reactions for conformers **2**−**4** are 1.3, −0.5, and 3.2 kcal/mol relative to that of **1**, respectively.

B. Mechanism of the Reaction. Generation of Active Catalyst. As mentioned in the Introduction, the cation−olefin cyclization is initiated by a η^2 metal−olefin complex in the presence of base (Ph_2NMe) and ambient CH_2Cl_2 as solvent. Since the catalyst has only one obvious vacant site to make a square-planar coordination environment, substrate (olefin), solvent (CH_2Cl_2), and base (Ph_2NMe) were expected to compete for coordination to this vacant site. To better explore this, we calculated the binding energy between **(**$PPP)Pt^{2+}$ and L, where L = NMe_3, CH_2Cl_2, CH_2═CH_2, CH_2═CHMe (for asymmetry). As shown in Table 2, the L−$(PPP)Pt^{2+}$ binding energies (negative values indicating binding) are −60.0 (−47.3), −28.2 (−18.0), −36.4 (−24.6), and −41.0 (−27.9) kcal/mol for L = NMe_3, CH_2Cl_2, CH_2═CH_2, CH_2═CHMe, respectively. In other words, NMe_3 binds to the catalyst more strongly than solvent or substrate by 20−30 kcal/mol (consistent with the need for a bulky poor base such as Ph_2NMe in the experimental protocol). Meanwhile, substrate binds to the catalyst about 5−15 kcal/mol more strongly than CH_2Cl_2, making it the thermodynamically favored ligand under the reaction conditions.

The calculations show that $(CH_2$═$CH_2)(PPP)Pt^{2+}$ and $(CH_2$═CHMe$)(PPP)Pt^{2+}$ complexes may have two different isomers, coplanar (**Iso-1**) and out of plane (**Iso-2**). For the small catalyst model (where phenyl groups of the real catalyst are replaced by hydrogen atoms), the two isomers of $(CH_2$═$CH_2)(PPP)Pt^{2+}$ have similar energies; **Iso-2** is 1.1 (0.4) kcal/mol less stable than **Iso-1.** These two isomers are separated from each other by a small barrier of 0.9 (1.8) kcal/mol (calculated from **Iso-1**) associated with rotation of the CH_2═CH_2 fragment. For the large model catalyst (with PPh_2 groups) the energy difference between these two isomers is reduced to 0.6 (−0.5) kcal/mol. The barrier separating these two isomers is expected to be smaller (less than 1 kcal/mol) and has not been calculated.

For the bulkier olefin $(CH_2$═CHMe$)(PPP)Pt^{2+}$, the energy difference between the **Iso-1** and **Iso-2** isomers is reversed: the out-of-plane isomer (**Iso-2**) is slightly more stable than the coplanar isomer (**Iso-1**) by 0.6 and 0.1 kcal/mol by utilizing small and large catalyst models, respectively. Due to the steric effect, the positions of the phenyl groups are slightly different in the two coplanar and out-of-plane isomers. For the bulkier $(CH_2$═CHMe$)(PPP)Pt^{2+}$, the dihedral angles P−Pt−P−Ph of two phenyl groups are changed by ca. 9° between the two isomers. The analogous difference is about 5° for the smaller CH_2═CH_2 adduct.

Comparing the geometries of adduct complexes for the small and large catalyst models (see Figure 3), one notices that in the large model catalyst, the C−C bond lengths of Pt−CH_2═CH_2

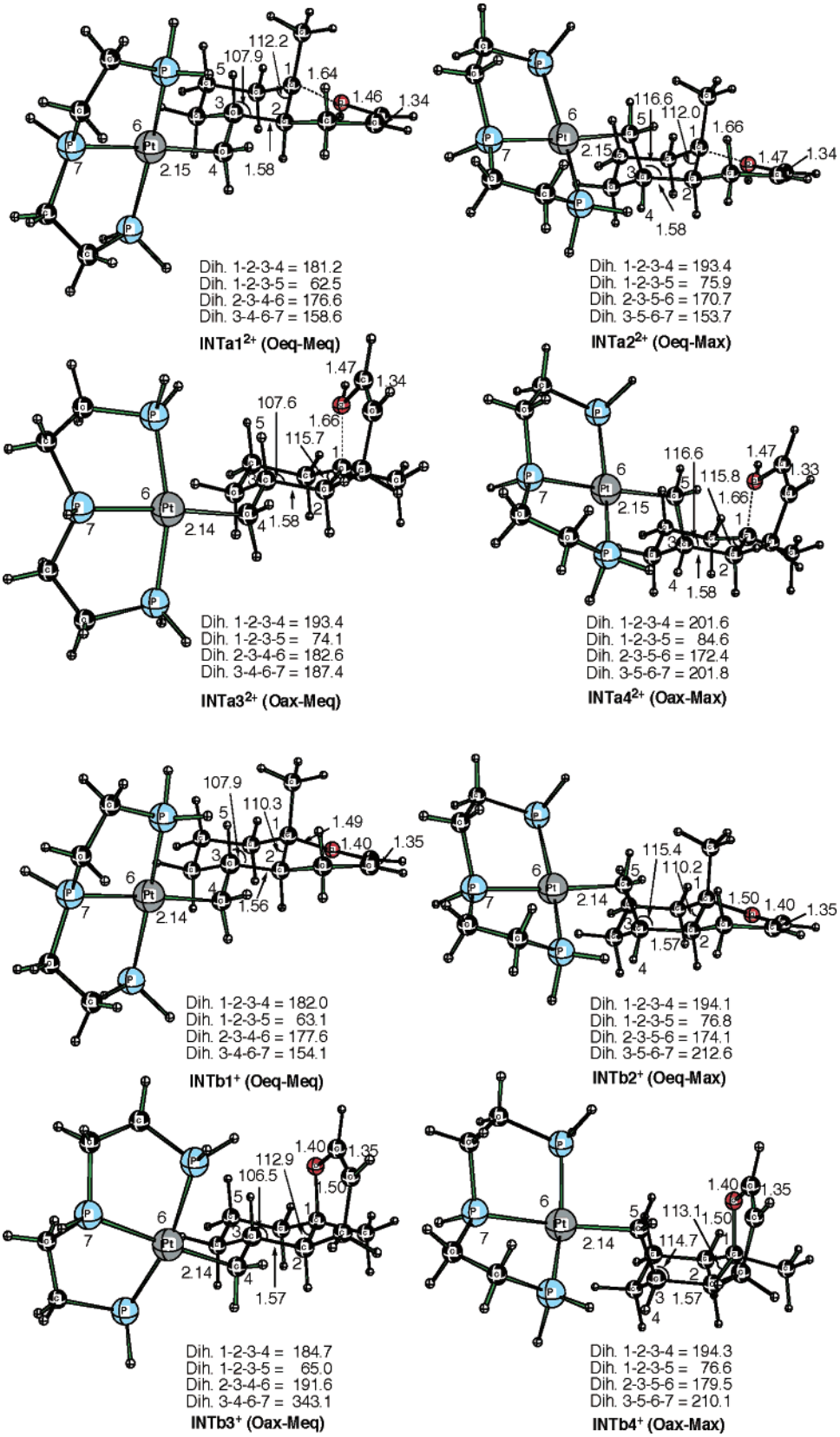

Figure 2. Calculated geometrical structures (with bond distances in Å) of the four different diastereoisomers of the intermediates **INTa**$^{2+}$ and **INTb**$^{+}$. The number 5 always refers to the axial position, regardless of the atom type.

and the Pt−P distance trans to CH_2═CH_2 are smaller by 0.04 and 0.02 Å, respectively, while the two Pt−P_{cis} distances are larger by 0.03−0.05 Å. The calculated structure of the CH_2═CHMe adduct of the small model indicate an asymmetry in the Pt−C bond lengths, with the Pt−CH_2═CHMe and Pt−CHMe═CH_2 bond lengths being 2.37 and 2.56−2.57 Å, respectively. Interestingly, for the large model the Pt−CH_2 distance essentially remains the same, while the Pt−CHMe distance shrinks to 2.52 Å. As a result of the bonding asymmetry, the electron density on the internal carbon changes to −0.02e. compared to

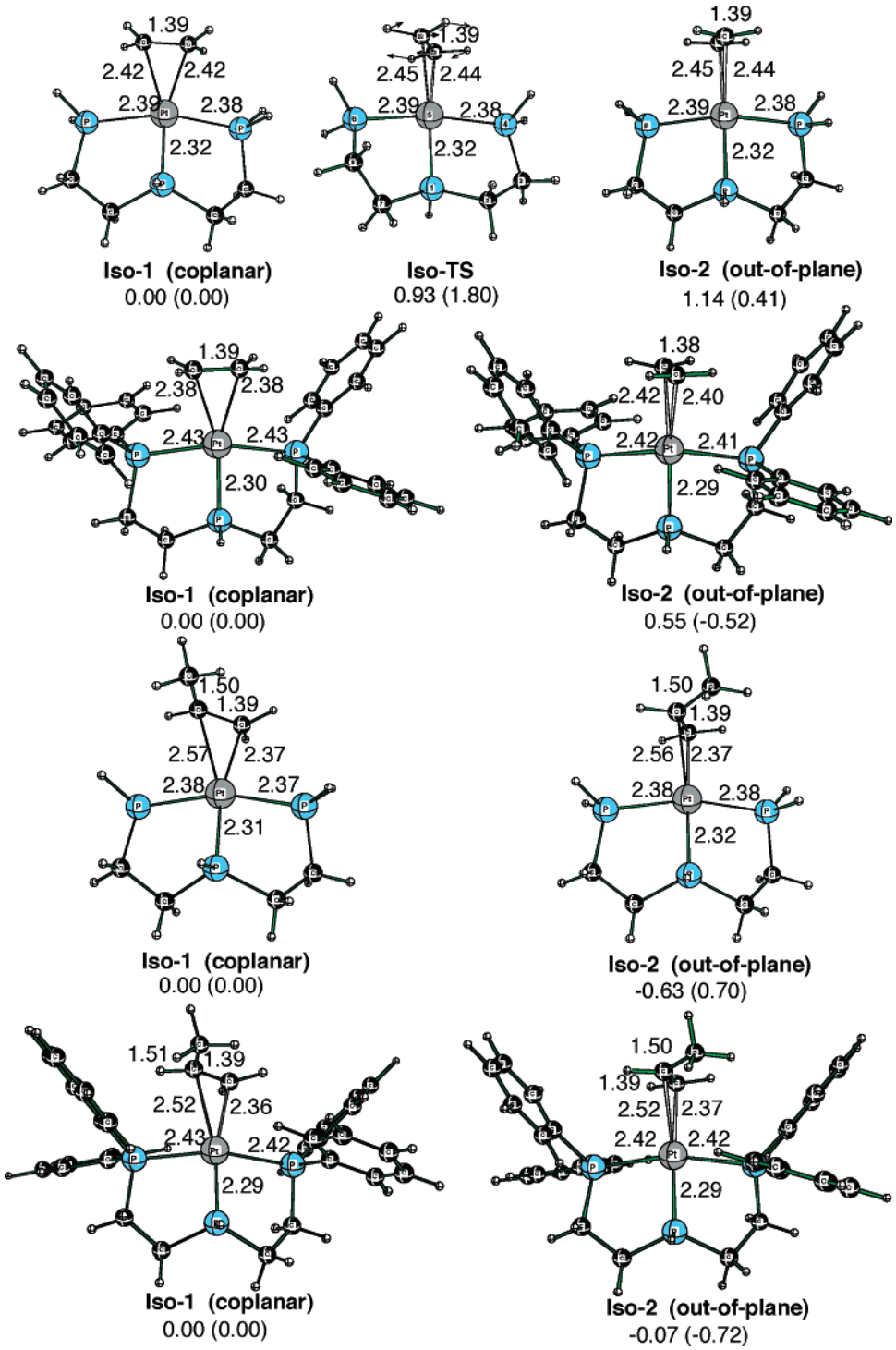

Figure 3. Relative energies and calculated geometrical structures (with bond distances in Å) of the two isomers **Iso1** (coplanar) and **Iso2** (out of plane) for $(CH_2{=}CH_2)(PPP)Pt^{2+}$ and $(CH_2{=}CHMe)(PPP)Pt^{2+}$ complexes utilizing model and real catalyst.

Table 2. L−(PPP)Pt^{2+} Binding Enthalpy and Gibbs Free Energies (in Parentheses) in kcal/mol at 298.15 K and 1 atm for Different Ligands L[a]

	L			
	NMe_3	CH_2Cl_2	$CH_2{=}CH_2$	$CH_2{=}CHMe$
E_{Stab}(L−(PPP)Pt^{2+})	−60.03 (−47.26)	−28.19 (−18.04)	−36.42 (−24.60)	−40.98 (−27.87)

[a] Negative values indicate binding.

+0.1e for the terminal carbon. The corresponding charges in the PCM optimized structures are +0.09e and −0.01e, respectively. In the case of the symmetric ethylene structure, the charges are +0.07e and +0.09e for the gas phase and PCM model, respectively.

Thus, the aforementioned results indicate that both coplanar (**Iso-1**) and out-of-plane (**Iso-2**) isomers of $(CH_2{=}CH_2)(PPP)Pt^{2+}$ and $(CH_2{=}CHMe)(PPP)Pt^{2+}$ are energetically feasible. However, the energy difference between them and the energy barrier separating these isomers are small. We have chosen the out-of-plane structure as a starting point for our further studies.

Pt-Mediated Cyclization of 1,6-Dienylphenol. After the detailed discussion on the structure and relative stabilities of the isomeric intermediates and products in section A, as well as an exploration of the nature of possible catalysts in section

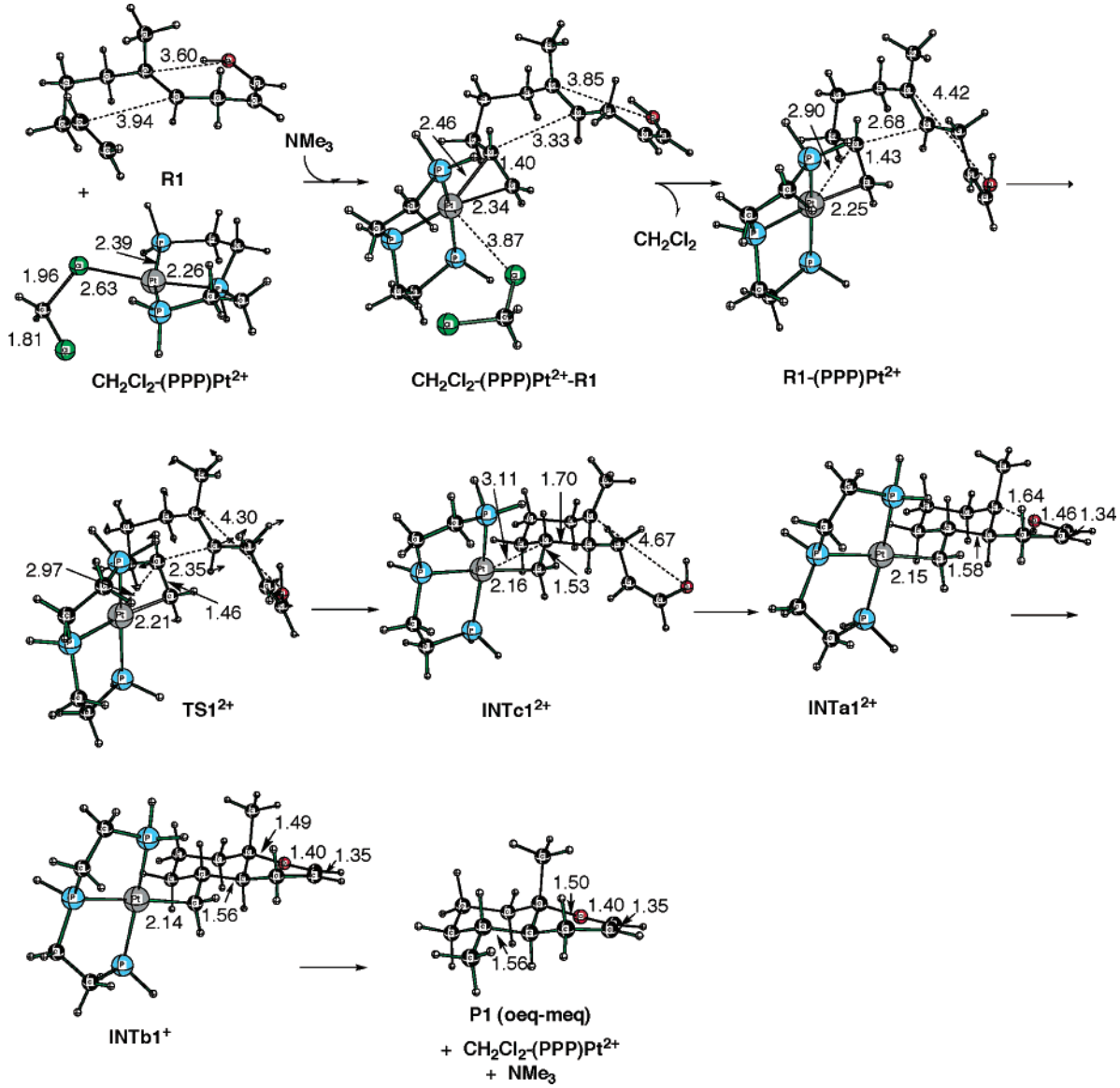

Figure 4. Calculated geometrical structures (with bond distances in Å) of the key species for platinum-catalyzed cyclization of 1,6-dienylphenol leading to the major product **P1**.

B, in this subsection we analyze the gas-phase potential energy surface for the platinum-mediated cyclization of 1,6-dienylphenol to the major product **P1**, using the small catalyst model and substrate. The optimized structures for the key intermediates and transition state of this reaction are shown in Figure 4, and the corresponding potential energy surface is presented in Figure 5.

The initial step of the reaction is substrate coordination to the transition-metal center of the catalyst **(CH$_2$Cl$_2$)(PPP)Pt^{2+}** to form the five-coordinate intermediate **(CH$_2$Cl$_2$)(PPP)Pt^{2+}R1,** which is stable by 25.8 (15.3) kcal/mol relative to **(CH$_2$Cl$_2$)-(PPP)Pt^{2+}** + **R1** dissociation limit. However, the resulted complex can easily (requiring only 5.5 kcal/mol in enthalpy and is even exothermic by 3.2 kcal/mol in free energy) dissociate the solvent molecule CH_2Cl_2 to give the four-coordinated **R1-(PPP)Pt^{2+}**, which we adopt to be the prereaction complex of the entire catalytic process. One should note that the dissociation of the solvent molecule from **(CH$_2$Cl$_2$)(PPP)Pt^{2+}**, without help from the coming substrate, is calculated to be exothermic by 28.2 (18.0) kcal/mol.

The next step of the reaction is cyclization, which starts from **R1(PPP)Pt^{2+}** and may proceed through a stepwise or concerted pathway. The stepwise pathway starts with nucleophilic attack on the activated alkene, goes through the transition state **TS1^{2+}** with a 2.2 kcal/mol Gibbs free energy barrier,[23] and leads to the key intermediate **INTc^{2+}** (obtained from a pseudo-IRC calculation from **TS1^{2+}**). As shown in Figure 4, **TS1^{2+}** has only one imaginary frequency of 75*i* cm^{-1}, which corresponds to the C−C bond closure leading to carbocyclic ring formation. The C−C bond distance is reduced from 2.35 Å in **TS1^{2+}** to 1.70 Å in **INTc^{2+}**. The formation of **INTc^{2+}** is thermoneutral in Gibbs free energy. The trapping of enol could occur on either face of this complex; trapping from the bottom face leads to a trans ring junction (**INTa1^{2+}**), while it leads to a cis ring junction (**INTa3^{2+}**) from the top face.

Rearrangement of **INTc^{2+}** to **INTa1^{2+}** completes the carbocyclic ring closure. The shrinkage of the C−O bond (with

(23) The calculated enthalpy for **R1(PPP)Pt^{2+}** is 0.4 kcal/mol higher than that for **TS1^{2+}**. This unrealistic reversed energy is caused after addition of enthalpy correction. The total electronic energy is lower by 0.09 kcal/mol. The IRC reversed calculation also indicates the connectivity between the structures, although continuing the IRC reversed calculation will eventually lead to a structure where enol is rotated toward and is hydrogen bonded to the PH_2 ligand of the metal. Obviously, this structure is an artifact of modeling PPh_2 as PH_2 and is not relevant to the reaction coordinate.

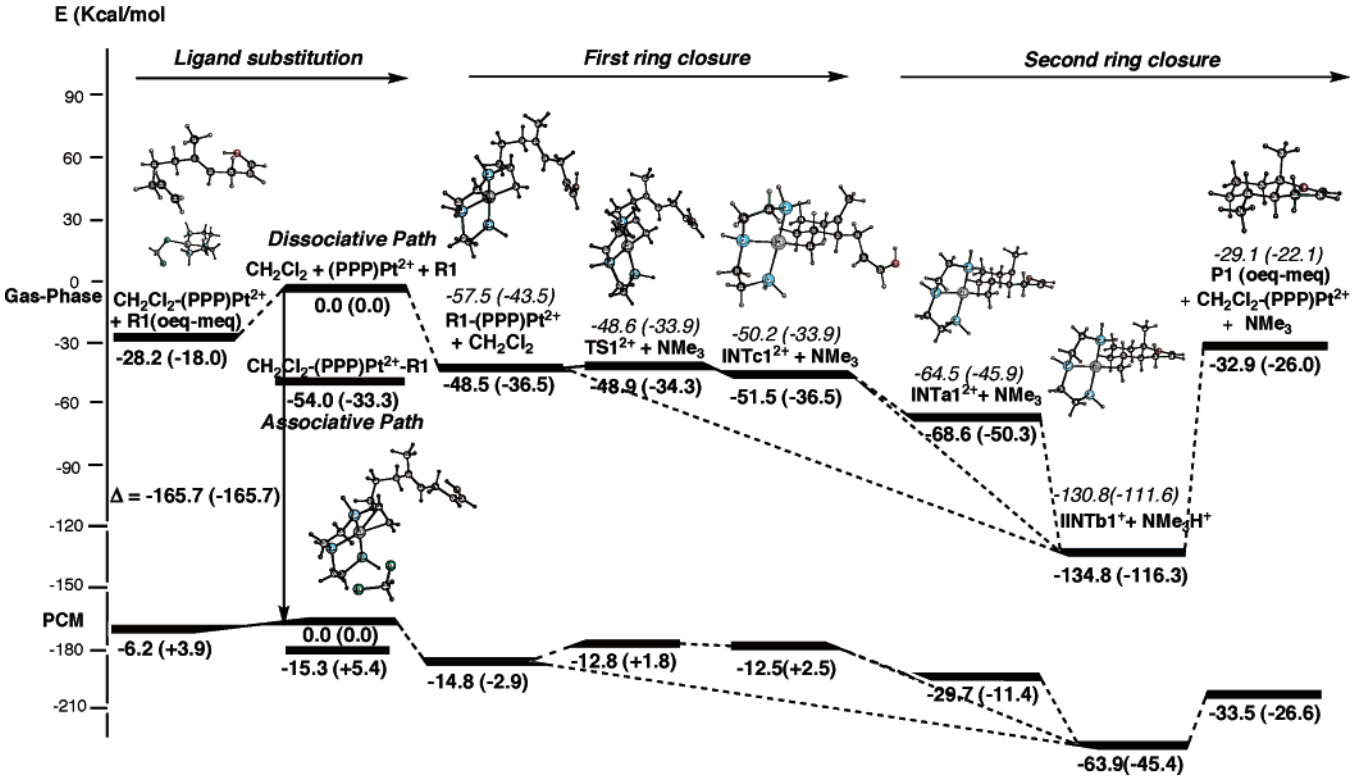

Figure 5. Δ*H* scaled potential energy profile of platinum-catalyzed cyclization of 1,6-dienylphenol leading to the major product **P1** both in the gas phase and in solution (boldface) and leading to the minor product **P2** (italics). Δ*G* values are given in parentheses.

Table 3. One-Dimensional Relaxed Scan for Fixed N−H Bond Following the Path $INTa1^{2+}$ → $INTb1^{+}$ [a]

complex	N−H (Å)	O−H (Å)	C−O (Å)	C−C (Å)	*E* (kcal/mol)
reactant	∞	0.98	1.62	1.57	0.00
scan point 1	1.9 (fixed)	1.04	1.58		−32.09
scan point 2	1.7 (fixed)	1.07	1.57		−37.40
scan point 3	1.5 (fixed)	1.15	1.56		−43.36
scan point 4	1.3 (fixed)	1.33	1.54		−50.92
scan point 5	1.1 (fixed)	1.63	1.53		−58.91
product	bond[b]	∞	1.49	1.58	−68.68

[a] The reactant and product are fully optimized. [b] The proton migrated to NMe_3, and NMe_3H^+ is formed.

Table 4. Three-Dimensional Relaxed Scan for Fixed N−H, O−H, and C−O Bonds Following the Path $INTc1^{+2}$ → $INTb1^{+}$ [a]

complex	N−H (Å)	O−H (Å)	C−O (Å)	C−C (Å)	*E* (kcal/mol)
reactant	∞	0.98	4.67	1.70	0.00
scan point 1	3.00 (fixed)	1.00 (fixed)	3.00 (fixed)	1.65	−19.89
scan point 2	3.00 (fixed)	1.00 (fixed)	2.30 (fixed)	1.62	−23.69
scan point 3	3.00 (fixed)	1.00 (fixed)	1.90 (fixed)	1.59	−28.16
scan point 4	3.00 (fixed)	1.00 (fixed)	1.50 (fixed)	1.57	−30.63
scan point 5	1.90 (fixed)	1.40 (fixed)	1.50 (fixed)	1.57	−30.82
scan point 6	1.50 (fixed)	1.80 (fixed)	1.50 (fixed)	1.56	−42.81
scan point 7	1.10 (fixed)	3.00 (fixed)	1.50 (fixed)	1.56	−67.08
product	bond[b]	∞	1.49	1.56	−87.05

[a] The reactant and product are fully optimized. [b] The proton migrated to NMe_3, and NMe_3H^+ is formed.

distance 4.67 Å in $INTc^{2+}$ to 1.64 Å in $INTa1^{2+}$) as well as the shrinkage of the C−C bond to 1.58 Å makes the $INTc^{2+}$ → $INTa1^{2+}$ rearrangement exothermic by 17.1 (13.8) kcal/mol. We could not locate a transition state associated with the $INTc^{2+}$ → $INTa1^{2+}$ rearrangement. However, on the basis of our careful scan for C−O and C−C bond formation (discussed below), we believe that when amine is in the vicinity of the hydroxyl group, the isomerization occurs without a barrier. Obviously, this will not be the case for the isomerization of $INTc3^{+2}$ to $INTa3^{2+}$, where significant reorganization is necessary for the phenol to add to the top face of the cation. This is also in agreement with the experimental data, where stereoisomer **3** has not been detected in the reaction. Thus, we believe that in the presence of base the overall reaction is concerted, though not necessarily synchronous. Similar conclusions were drawn from previous computational studies[9−11] examining the steroidal cascade reaction.

From the resultant intermediate $INTa1^{2+}$, the reaction proceeds via amine-assisted proton abstraction to the monocationic complex $INTb1^{+}$, where hetero ring formation is complete. The major geometrical differences between $INTa1^{2+}$ and $INTb1^{+}$ are the C−O bond shortening (1.64 to 1.49 Å) and shrinkage of the adjacent C−C bond from 1.46 to 1.40 Å.

The deprotonation coupled with C−O bond shrinkage is a downhill concerted process. We performed a one-dimensional relaxed scan by approaching amine to $INTa1^{2+}$. The structures are optimized while the N−H bond lengths are fixed at different values. The results given in Table 3 indicate that, as the amine approaches the hydroxyl group, the O−H bond stretches and the C−O bond distance decreases. These reduce the total electronic energy gradually to reach $INTb1^{+}$ with an exothermicity of 68.7 kcal/mol. We also carried out a three-dimensional relaxed scan (by fixing of N−H, O−H, and C−O distances) following the path from $INTc1^{+2}$ to $INTb1^{+}$ with the inclusion of amine in the reaction complex for deprotonation; this pathway *bypasses* the intermediate $INTa1^{2+}$ (see Table 4). The results indicate that as the O−H distance increases from 1.00 to 3.00 Å and the N−H and C−O distances decrease from 3.00 to 1.10 Å and from 4.67 to 1.49 Å, respectively, the energies of the optimized structures become lower, indicative of a downhill process with no barrier.

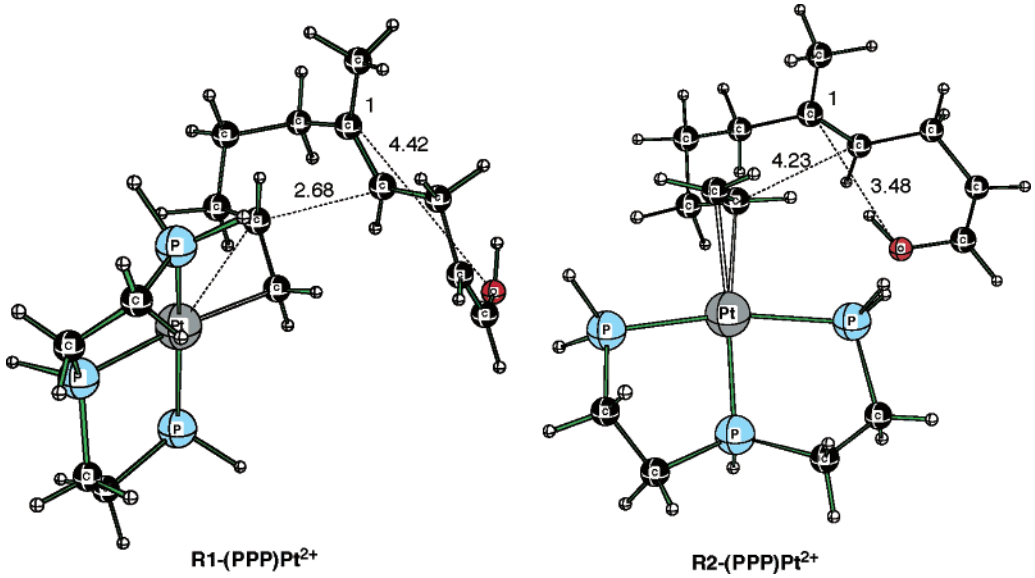

Figure 6. Calculated geometrical structures (with bond distances in Å) of the small models **R1(PPP)Pt**$^{2+}$ and **R2(PPP)Pt**$^{2+}$ showing the position of the trapping enol group.

Table 5. Two-Dimensional Relaxed Scan for Various Fixed C−O and C−C Bonds (While Assuming Proton is Fixed between N and O), Following the Path R1(PPP)Pt^{2+}→ INTb1^{+} [a]

complex	N−H (Å)	O−H (Å)	C−O (Å)	C−C (Å)	*E* (kcal/mol)
reactant	∞	0.98	4.72	3.20	0.00
scan point 1	1.50 (fixed)	1.80 (fixed)	3.00 (fixed)	1.85 (fixed)	3.21
scan point 2	1.50 (fixed)	1.80 (fixed)	2.30 (fixed)	1.70 (fixed)	−10.87
scan point 3	1.50 (fixed)	1.80 (fixed)	1.90 (fixed)	1.55 (fixed)	−27.20
product	bond[b]	∞	1.49	1.58	−84.23

[a] The reactant and product are fully optimized. [b] The proton migrated to NMe_3, and NMe_3H^+ is formed.

Another possible path for the reaction is a concerted mechanism for ring closure and deprotonation: i.e., a direct path from **R1(PPP)Pt**$^{2+}$ to the final intermediate **INTb1**$^{+}$. Despite our efforts, we could not find a transition-state structure on the fully concerted pathway. Therefore, we explored the potential energy surface, applying a two-dimensional relaxed scan for various fixed values of C−O and C−C distance (see Table 5), while assuming the proton to be fixed between O and N atoms with O−H = 1.8 Å and N−H = 1.50 Å. The energy of optimized structures decreased when the C−C and C−O distances were shortened from 1.85 to 1.55 Å and from 3.00 to 1.90 Å, respectively. Although the scan was limited, this is strongly suggestive of *a downhill path directly connecting **R1(PPP)-Pt**$^{2+}$ to the final intermediate **INTb1**$^{+}$*. A similar result was obtained when the scan was performed using the large catalyst.

In the light of the above results, we conclude that the most probable path is the concerted mechanism, wherein deprotonation and cyclization occur concurrently without barrier, thus bypassing the carbocationic intermediates **INTc1**$^{+2}$ and **INTa1**$^{2+}$; the existence of these latter intermediates seems only relevant in the absence of an amine base.[4,5]

We also studied the potential energy surface for the platinum-mediated cyclization of 1,6-dienylphenol to **P2**, which is the minor product in the experiment. The optimized geometries are provided in Figure S3 of the Supporting Information, and the relative energies are shown in Figure 5. A comparison of the energetics of the analogous structures of isomers **1** and **2** indicates that isomer **1** is more stable in general. The major exception is **R2(PPP)Pt**$^{2+}$, which is 12.2 (8.6) kcal/mol more stable than **R1(PPP)Pt**$^{2+}$. Interestingly, the structural differences between these two isomers are not limited to the position of the CH_2Pt group (as was the case in the initial structures for optimization), which is in a pseudo-equatorial position in **R1(PPP)Pt**$^{2+}$ and in a pseudoaxial position in **R2(PPP)Pt**$^{2+}$. As shown in Figure 6, the enol in **R2(PPP)Pt**^{2} is now rotated toward the metal. We also tried optimization utilizing a frozen dihedral angle; however, the same **R2(PPP)Pt**$^{2+}$ structure is obtained after releasing the constraint. According to our current calculation results, it seems that the cyclization from **R2(PPP)Pt**$^{2+}$ to **INTb2**$^{+}$ is not downhill, since the enol needs to rotate further toward carbon 1 (compared to the cyclization from **R1(PPP)-Pt**$^{2+}$ to **INTb1**$^{+}$). This is in agreement with the experimental data on the reaction selectivity for isomer **1**. Nevertheless, more detailed analysis utilizing the large catalyst and reactant models may be necessary to fully understand the diastereoselectivity of the reaction.

C. Effects of the Bulk Solvent. We studied the bulk solvent effects on the calculated energetics of the cyclization. The energies of reactants, transition state, intermediates, and products of the reaction path leading to **P1** were evaluated with the polarizable continuum model (PCM) by utilizing the gas-phase optimized geometries and dichloromethane as a solvent media. The PCM-calculated energies for isomer **1** along the entire potential energy surface of the reaction are compared with the corresponding gas-phase values in Figure 5. Although the inclusion of solvent effects does not change the general trend obtained in the gas-phase studies, it stabilizes the separate reactants more than the intermediate structures and transition states, and, consequently, makes the solvent−substrate substitution less exothermic.

In the presence of solvent, the concerted path seems to be still downhill and favorable, while the first ring closure in the stepwise path needs almost the same activation energy of 2.0 (1.1) kcal/mol as in the gas phase. Addition of zero-point energy, enthalpy, and entropy corrections of the gas-phase studies to the PCM-calculated enegetics does not change the shape of the potential energy surface (PES), except for the relative position of **INTc1**$^{+2}$ on the PES. The **INTc1**$^{+2}$ is located 0.7 kcal/mol lower than **TS1**$^{2+}$ at the PCM level without zero-point energy or thermal enthalpy and entropy corrections; however, with the

enthalpy and the free energy it is higher in energy than **TS1**$^{2+}$ by 0.3 and 0.7 kcal/mol, respectively.

4. Conclusions

From the results and discussion presented above, we can summarize our conclusions as follows.

1. Among four different diastereomers for **P**, **INTb**$^{+}$, and **INTa**$^{2+}$, the isomer **1 (Oeq-Meq)** is found to be the energetically most stable one, which is consistent with the available experimental results.

2. The bicyclization of **R1** takes place without a significant activation barrier. By using the small model catalyst we have shown that the concerted mechanism for bicyclization and deprotonation of **R1(PPP)Pt**$^{2+}$ is a barrierless and energetically downhill process and leads to the **INTb1**$^{+}$ product. A stepwise path proceeds with a small barrier of 2.0 (1.1) kcal/mol (in solution) at **TS1**$^{2+}$ and leads to the first ring closure intermediate **INTa**$^{2+}$, which transforms to the bicyclic intermediate **INTb1**$^{+}$ by closing of the second ring with the help of the amine fragment. The use of the large model catalyst (including four phenyls) for the concerted pathway from **R1(PPP)Pt**$^{2+}$ to **INTb1**$^{+}$ leads to the same conclusion. Therefore, it is most likely that the bicyclization of 1,6-dienylphenols proceeds concertedly with no significant barrier in the presence of base; the stepwise path involving a free carbocationic intermediate seems to be less favorable.

3. The major structural difference between **R2(PPP)Pt**$^{2+}$ and **R1(PPP)Pt**$^{2+}$ complexes is the position of the trapping enol group. The positioning of this enol group could be an explanation for why **P2** is the experimental minor product, though additional studies on the fully elaborated structures may be needed to fully explain this.

4. The calculations that include the bulk solvent effect using the polarizable continuum model (PCM) do not change the conclusion obtained for the gas-phase results for the present bicyclization of 1,6-dienylphenol.

Acknowledgment. The present research was supported in part by a National Science Foundation grant (No. CHE-0209660). M.R.G. gratefully acknowledges the National Institutes of Health for support (No. GM-60578). The computer facilities are supported in part by a DURIP grant (No. FA9550-04-1-0321) from the AFOSR. The use of computational resources at the Cherry Emerson Center for Scientific Computation is also acknowledged.

Supporting Information Available: Figure S1, giving the calculated geometrical structures (with bond distances in Å) of the four different diastereoisomers of the product **P-Large**, Figure S2, giving the calculated geometrical structures (with bond distances in Å) of the four different diastereoisomers of the reactant **R**, Figure S3, giving the calculated geometrical structures (with bond distances in Å) of the key species for platinum-catalyzed cycloisomerization of 1,6-dienylphenol leading to the minor product **P2**, and Table S4, giving Cartesian coordinates of all structures reported in this paper. This material is available free of charge via the Internet at http://pubs.acs.org.

OM060632F